

USE OF X-RAY COMPUTED TOMOGRAPHY AS INPUT FOR FRACTURE MODELLING OF CEMENT PASTE-AGGREGATE INTERFACE

H. ZHANG*, E. SCHLANGEN[†] AND B. ŠAVIJA[‡]

*Delft University of Technology
Delft, The Netherlands
e-mail: h.zhang-5@tudelft.nl

[†]Delft University of Technology
Delft, The Netherlands
e-mail: erik.schlangen@tudelft.nl

[‡]Delft University of Technology
Delft, The Netherlands
e-mail: b.savija@tudelft.nl

Key words: X-ray computed tomography, Interface microstructure Lattice model, Mechanical properties

Abstract. This work aims to investigate the mechanical properties of the cement paste-aggregate interface by combining experimental and numerical approaches. The multi-phase interface microstructure was obtained by X-ray computed tomography (XCT) and submitted to a discrete fracture lattice model for fracture analysis. Apart from the modelling, a benchmark test at the micro-scale has been conducted for the purpose of calibration. With the approach proposed in this work, a framework to model and test the micromechanical properties of the cement paste-aggregate interface at the micro-scale has been formed.

1 INTRODUCTION

Concrete is generally considered to be a three-phase material composed of aggregate, cement paste matrix and the ITZ at meso-scale. In order to offer fundamental insight into the fracture mechanisms of such composite material and give a proper prediction, the input parameters of each phase are required to be calibrated separately. The behaviour of the matrix phase and the aggregate can be studied in a rather straightforward manner because these materials can be prepared and tested individually. However, this does not apply to the ITZ, because this zone is an integral part of the whole microstructure together with the bulk cement paste and the aggregate.

Over the past decades, various test configurations have been developed to study the interface fracture. The specimens are generally made by casting the cementitious matrix against a flat block of aggregate. Load is then applied to split these two materials along the interface to quantify the bonding strength. Because almost all fracture experiments are carried out at the scales larger than that of real aggregate in concrete and ITZ is a special material feature at the micro-scale, a clear understanding about the micromechanical properties of the ITZ is still missing. At the micro-scale, studies are mostly carried out by simulations [1,2] due to the technical and instrumental limitations. These models can hardly be validated because of the mis-

match in terms of the investigated scale length. Consequently, there remains a need for experimental measurements at the micro-scale, which can set a benchmark for the calibration and validation of the micromechanical modelling of the ITZ.

In this work, small hardened cement paste (HPC) cantilevers with one end attached to the aggregate were produced by micro-dicing and tested using nanoindenter. Besides of the experiments, a micromechanical model of ITZ is proposed. The model is built up on the basis of a combination of X-ray computed tomography and discrete lattice fracture model. As the size of specimens that considered in the modelling and experiments are identical, the experimental measurements can be used for the calibration of the numerical model.

2 Mechanical test

A strip of aggregate consisting of a row of HPC cantilevers (Figure 1) was produced by running a micro-dicing saw over the surface of a HPC-aggregate slice. The measurements show that the HPC cantilevers have a length of $200\ \mu\text{m}$ and a cross-section of $100\ \mu\text{m} \times 100\ \mu\text{m}$.

The test configuration is schematically shown in Figure 2. The aggregate strip was bonded to a support vertically resulting in a row of HPC cantilevers standing horizontally. A nanoindenter was then instrumented for applying load at the free end of the cantilever using a commercialised flat end cylindrical tip with a diameter of $330\ \mu\text{m}$. The tip was set to be aligned with the centre of the free end of the beam using an in-situ imaging system. The test was run under a displacement-controlled method with a constant displacement increment of $50\ \text{nm}$ per second. The cantilever beams were loaded until failure and the load-displacement curves were recorded by the nanoindenter for further analysis.

In total, 10 cantilever beams were tested. Figure 3 shows their load-displacement curves. A good repeatability can be found and, in general, these curves can be divided into two parts: ascending and plateau. In the ascending part,

the load increases monotonically with the displacement until reaches a critical load. Afterwards, a displacement jump is observed. This is because the control of the nanoindenter is not fast enough to enable a stable post-peak behaviour measurement. Consequently, a catastrophic failure happens and the indenter overshoots downward. Thus, only the first regime was used for the calibration of the fracture model.

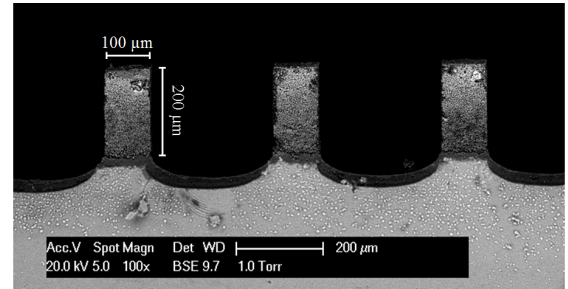


Figure 1: Environmental scanning electron microscope image of prepared cantilever beams.

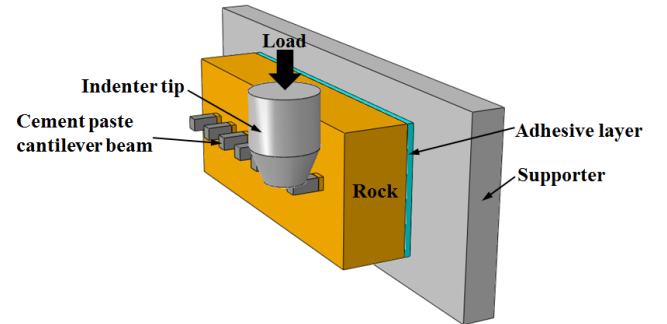


Figure 2: Schematic view of the test setup.

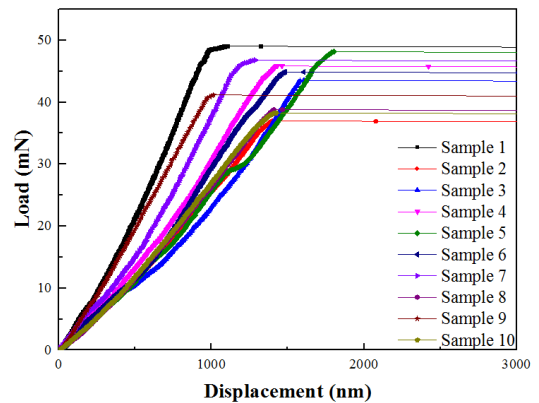


Figure 3: Experimental load-displacement diagrams of the mechanical tests.

3 Interface characterisation

3.1 XCT experiments

The fracture modelling requires virtual specimen with details of the featured material structure. In this work, XCT and image segmentation techniques were used to characterize the interface structure and build the digital specimen which is comparable with the realistic specimen. As shown in Figure 4: a HPC-aggregate prism was created and clamped on a special holder for the scanning. A small drop of cyanoacrylate adhesive was added to the surface of the specimen for the purpose of protection of the sample from broken during clamping. The prism has a square cross-section of $500 \mu\text{m} \times 500 \mu\text{m}$ and a length of 3 mm.

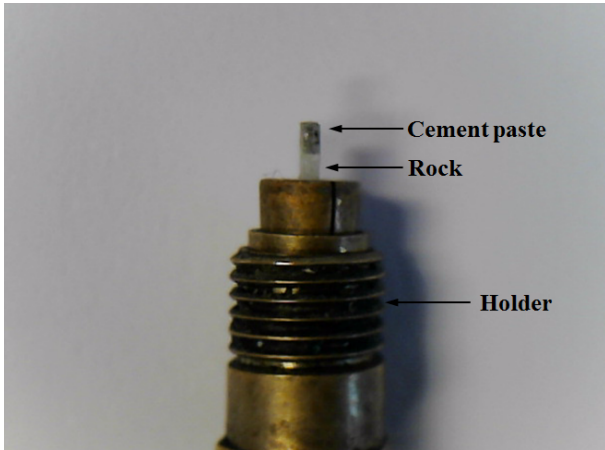


Figure 4: HPC-aggregate specimen clamped on the holder for XCT scanning.

In the XCT experiment, the holder was fixed in the rotatable stage. The X-ray source tube was set as 120 Kev/60 μA for the scanning. 2800 projections were acquired using a digital GE DXR detector (3072×2400 pixels). This setup results in a greyscale-based material structure with a resolution of $1 \mu\text{m} \times 1 \mu\text{m} \times 1 \mu\text{m}$. In order to reduce the noise in the reconstructed XCT images as well as the computational efforts in the discrete fracture modelling, a binning level of 2 was used in the reconstruction. The resulting final material structure has a resolution of $2 \mu\text{m} \times 2 \mu\text{m} \times 2 \mu\text{m}$. Afterwards, a stack of 2D slices from the side view

was exported for image segmentation and digital specimen generation. To reduce the influence of beam hardening in the XCT experiment, a region of interest (ROI) with a cross-section of $300 \mu\text{m} \times 300 \mu\text{m}$ and length of $1000 \mu\text{m}$ was extracted from the central region of the scanned specimen.

3.2 Virtual specimen generation

First, the fluctuation of the greyscale level along the height of the ROI was analysed by calculating the coefficient of variation (CoV) of greyscale level of voxels at each row (same height) using:

$$\text{CoV}_i = \frac{S_i}{\mu_i} \quad (1)$$

where CoV_i is the CoV of greyscale level at row i , S_i the standard deviation greyscale level at row i , μ_i the mean greyscale level at row i . As shown in Figure 5, on the one hand, the CoV at the aggregate part is relatively low (below 0.1). On the other hand, cement paste has a much higher CoV. It is therefore reasonable to consider the aggregate as a single-phase material in the model. Additionally, a significant increase of CoV is observed at the boundary between aggregate and cement paste, which was used to separate the two materials from the original greyscale level-based images.

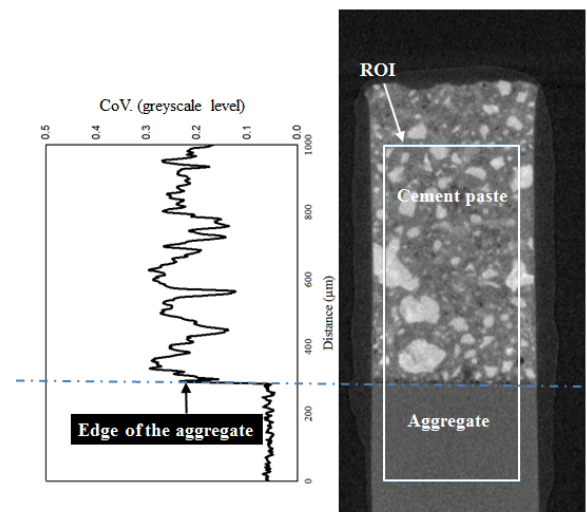


Figure 5: Fluctuation of the greyscale level along the ROI.

At the micro metre level, a multi-phase material structure of cement paste should be considered to model the fracture behaviour. Herein, a global thresholding approach that developed in the authors' previous work [3] was adopted to segment the cement paste part into a 4-phase material consisting of pore (P), inner hydration product (IHP), outer hydration product (OHP) and anhydrous cement particle (ACP). This method determines the threshold value of greyscale value using both cumulative and histogram of the greyscale level in the ROI. In order to avoid the influence of the ITZ on the determination of the threshold value of different phases, the region away from the edge of $150 \mu\text{m}$ was used, which can be regarded as the bulk cement paste.

A virtual specimen (Figure 6) having a cross-section of $100 \mu\text{m} \times 100 \mu\text{m}$ and length of $220 \mu\text{m}$ consisting of $20 \mu\text{m}$ length of aggregate and $200 \mu\text{m}$ length of HPC was extracted from the segmented voxel-based images for fracture analysis.

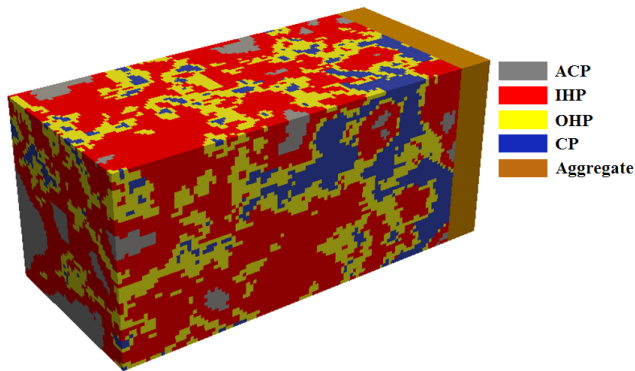


Figure 6: Virtual specimen with size of $220 \mu\text{m} \times 100 \mu\text{m} \times 100 \mu\text{m}$ ($110 \text{ voxel} \times 50 \text{ voxel} \times 50 \text{ voxel}$).

4 Modelling

A discrete lattice fracture model, as described in [3], was used to model the mechanical performance of the generated specimens. In total, 9 types of elements as listed in Table 1 were considered. For the elements that exist in the cement matrix, their mechanical properties have been calibrated and validated in the authors' previous works [3–5]. With respect to the

element within the aggregate, its elastic modulus is taken from [6]. The tensile strength is assumed as $1/1000$ of the modulus. The elements (Ag-I and Ag-O) that connect the solid phases in HPC and aggregate are assumed proportional to the phases they connect with in HPC. In this way, the elastic moduli and strengths of these elements can be calibrated through the inverse analysis using experimental measured load-displacement curves.

Table 1: Lattice element types and their assumed mechanical properties

Element type	Elastic modulus (GPa)	Tensile strength (MPa)
A-A	99	683
IHP	31	92
OHP	25	58
A-I	47	92
I-O	28	58
A-O	40	58
Ag-Ag	70	700
Ag-I	-	-
Ag-O	-	-

As schematically shown in Figure 7 and 8, the digital specimen has been mapped to a lattice mesh. The end of the aggregate part was clamped. In the experimental test, due to the rotation of the cantilever beam, the contact area between the flat end tip and the cantilever beam decreases gradually from fully contacted to only the edge of the indenter with the deformation of beam increasing. However, such dynamic boundary configuration could not be implemented. Two extreme boundary conditions were therefore adopted herein for the purpose of calibration. The fully contacted loading boundary condition was modelled by adding unit displacement at nodes within the dash line marked zone (Figure 7), while the edge contacted boundary condition was mimicked by applying unit displacement at the nodes at the right side edge (Figure 8). Through a trial-and-error approach, satisfactory load-displacement

curves were obtained when the values in Table 2 and 3 were adopted. As the fracture pattern for the simulated two boundaries are almost identical and a linear-elastic constitutive law is implemented for the local beam elements, the simulated load-displacement curves have similar shapes. Furthermore, The mechanical properties listed in Table 2 and 3 are rather low compared with the elements connecting phases in HPC. This tends to confirm the weak bonding between cement paste and aggregate. Figure 9 presents the comparison between the simulated load displacement curve and the experimental ones.

As mentioned above the experiments are not able to measure the post-peak behaviours, the comparison is only made in the pre-peak regime. Clearly, the simulation can reproduce the experimental measured results well in terms of the ascending slope and the peak load. The simulated fracture patterns at final stage are plotted in Figure 10. Almost all the interface elements are broken. While, the small amount unbroken interface element and the crack occurs in the HPC proves that there are some residual HCP left on the aggregate after the deboning. This is in accordance with the experimental observation.

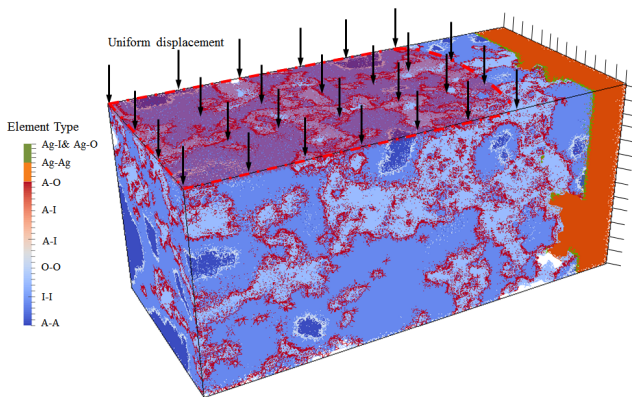


Figure 7: Schematic illustration of the boundary configurations for the modelling of the cantilever under loading: fully contacted with the indenter surface.

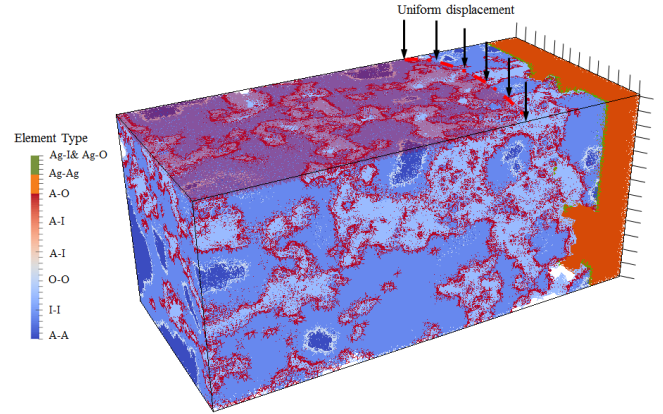


Figure 8: Schematic illustration of the boundary configurations for the modelling of the cantilever under loading: contacted with the edge of indenter.

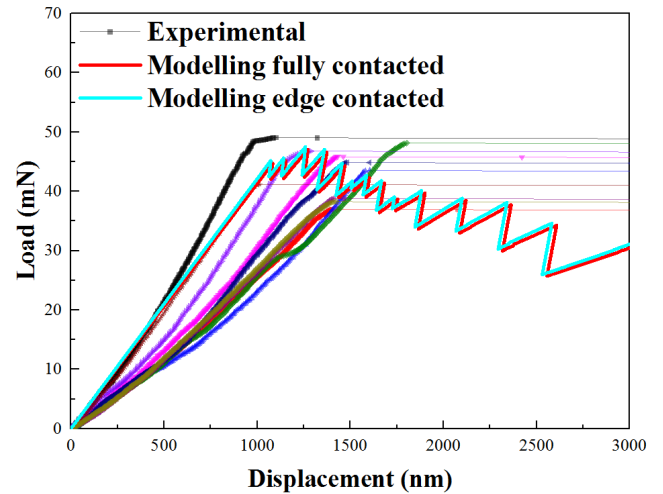


Figure 9: Fitting results of the lattice fracture model.

Table 2: Calibrated mechanical properties of the lattice elements connecting aggregate and HPC from fully contacted boundary conditions.

Element type	Elastic modulus (GPa)	Tensile strength (MPa)
Ag-I	0.2	3.0
Ag-O	0.16	2.5

Table 3: Calibrated mechanical properties of the lattice elements connecting aggregate and HPC from edge contacted boundary conditions.

Element type	Elastic modulus (GPa)	Tensile strength (MPa)
Ag-I	0.17	5.0
Ag-O	0.14	4.2

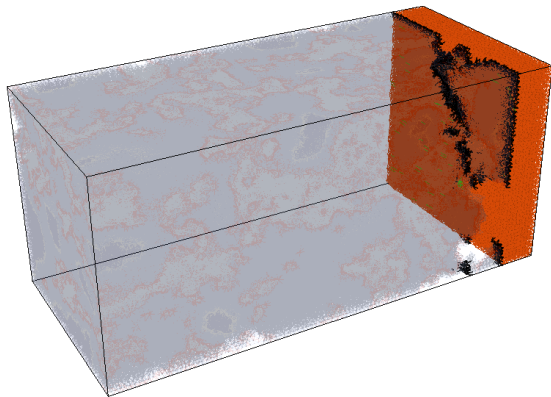


Figure 10: Simulated crack patterns at failure stage (black-crack).

5 CONCLUSIONS

This work proposes an approach for testing and modelling of HPC-aggregate interface at micrometre length scale. The micrometre sized HPC-aggregate cantilever beams are fabricated and tested both experimentally and numerically. The experimentally measured load-displacement responses are used as benchmark for the calibration of the numerical model. After calibration, the model can reproduce the experimental observations well. It is further used to explain the experiments in more detail.

REFERENCES

- [1] Garboczi, E. 1997. Stress, displacement, and expansive cracking around a single spherical aggregate under different expansive conditions. *Cement and Concrete Research* **27**:495–500.
- [2] Sun, Z. Garboczi, E.J. and Shah, S.P. 2007. Modeling the elastic properties of concrete composites: Experiment, differential effective medium theory, and numerical simulation. *Cement and Concrete Composites*, **29**:22–38.
- [3] Zhang, H., Šavija, B., Chaves Figueiredo, S., Lukovic, M. and Schlangen, E. 2016. Microscale testing and modelling of cement paste as basis for multi-scale modelling. *Materials* **9**:907.
- [4] Zhang, H., Šavija, B. Chaves Figueiredo, Stefan and Schlangen, E. 2017. Experimentally validated multi-scale modelling scheme of deformation and fracture of cement paste. *Cement and Concrete Research* **102**:175–186.
- [5] Zhang, H., Šavija, B. and Schlangen, E. 2018. Combined experimental and numerical study on micro-cube indentation splitting test of cement paste. *Engineering Fracture Mechanics* **199**:773–786.
- [6] Hassanzadeh, M. 1994. Fracture mechanical properties of rocks and mortar/rock interfaces. In Diamond et al (eds), *Microstructure of Cement-Based Systems/Bonding and Interfaces in Cementitious Materials*; pp.77-86.